7. T. Ido et al., J. Lightwave Technol., vol. 14 (1996), pp. 2026–2034.
8. M. Shirai et al., ECOC '00, vol. 1 (2000), pp. 45–46.
9. K. Takagi et al., OFC '01 (2001), paper MJ2.
10. H. Kawanishi, OFC '01 (2001), paper MJ3.
11. Y. Akage et al., Electron. Lett., vol. 37 (2001), pp. 299–300.
12. S. Kodama et al. UEO '01 (2001), pp. 92–94.
13. T. Ishibashi et al., UEO '97, vol. 13 (1997), pp. 83–87.
14. M. Yoneyama et al., Electron. Lett., vol 34 (1998), pp. 1607–1609.

WV2 **4:30 pm**

40 GHz Optical Pulse Generation using Traveling-wave Electroabsorption Modulator

Hsu-Feng Chou, Yi-Jen Chiu, and John E. Bowers, *Department of Electrical and Computer Engineering, University of California, Santa Barbara, Santa Barbara, CA 93106, USA, Email: hubert@ece.ucsb.edu*

1. Introduction

As bit rates per channel increase in modern optical communication systems, simple and stable optical pulse sources are needed because the RZ format is preferred at high bit rates.[1] Gain-switched lasers and mode-locked lasers have been frequently used as optical pulse sources. However, the former is subject to large frequency chirping and timing jitter while the later are more difficult to maintain and have problems in controlling the repetition cycles of the pulses. Electro-absorption (EA) modulators have been used to generate optical pulses with sinusoidal RF drive[2] and overcome these difficulties. The advantages of EA modulators include low-chirp, low jitter, and high-speed. However, high bias voltages and hence high driving powers are usually required to generate shorter pulses. Traveling-wave EA modulators (TWEAM) have been previously demonstrated in low driving power operation without sacrificing bandwidth.[3] In this work, we fabricated a multi-quantum-well (MQW) TWEAM to further improve the modulation efficiency and used it to generate optical pulses at 40 GHz repetition rate.

2. Fabrication and Characterization

An InGaAsP-based material grown by MOCVD is used to fabricate 330-μm long ridge-waveguide TWEAM. The active region consists of 10 tensile-strain wells and 11 compressive-strain barriers, modified from previous work.[3–5] Cladding layers of p-InP (top) and n-InP (bottom) are grown and sandwich the active region. After reactive-ion-etching (RIE), PMGI is utilized for passivating the etching surface of ridge waveguide. Fig. 1 shows the schematic diagram of the device. Two CPW lines forming the traveling-wave circuit are used as the microwave feed and load lines. The optical input and output ports are on the two cleaved and AR coated facets. Fig. 2 shows the TE and TM mode fiber to fiber transmission loss measurement at 1555 nm. A modulation efficiency of ~20 dB/V in the 0V to 2V reverse bias region and a total modulation depth of 47 dB are achieved.

3. Experiment and Results

For traveling-wave optical pulse generation, the TWEAM is terminated with a 50 Ohm load and driven with sinusoidal 5.6 Vpp microwave power. A 2 dBm 1555 nm CW laser is sent into the optical input port. As shown in Fig. 1, there are two configurations: (A) the optical wave propagates in the same direction as the microwave, which is termed as co-direction configuration, (B) the optical wave propagates in the direction opposite to the microwave propagation, which is termed as counter-direction configuration. The results for TM mode are shown in Fig. 3. The output power is measured after the TWEAM without amplification. It is obvious that there are different results for these two configurations, as expected for traveling wave modulators and not expected for lump-type modulators. The co-direction configuration gives about 4 dB higher output power than the counter-direction configuration. It also generates the shortest pulse, which is about 4 ps for the current setup. The difference in power can be explained by the fact that in the co-direction configuration the peak of the optical wave propagates with the peak of the microwave, which reduces the absorption in the QW by reducing the reverse bias locally. The velocity mismatch between optical- and micro- waves is not profound for the current device length.

To further investigate the traveling-wave behavior, a theoretical model based on transmission line theory has been developed, taking into account the temporal and spatial microwave and optical wave interaction via the transmission curve in Fig. 2. The only adjustable parameter in the model is the microwave coupling loss. The theoretical results are plotted in Fig. 4. The close agreement between the theoretical and experimental results supports the traveling-wave operation of the device.

The spectrum and the autocorrelation trace for the co-direction configuration at 1V reverse bias are shown in Fig. 5. The chirping property is studied by measuring the spectrum and time bandwidth product $\Delta\omega \cdot T_o$, where $\Delta\omega$ is the spectrum half-width at $1/e$ intensity point and T_o is the time-domain half-width at $1/e$ intensity point. The product for a transform-limited pulse is unity. The product as a function of reverse bias

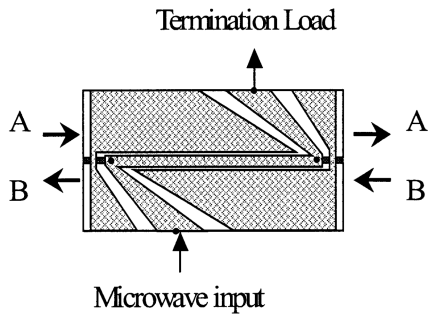

WV2 Fig. 1. Schematic diagram of TWEAM A: co-direction, B: counter-direction.

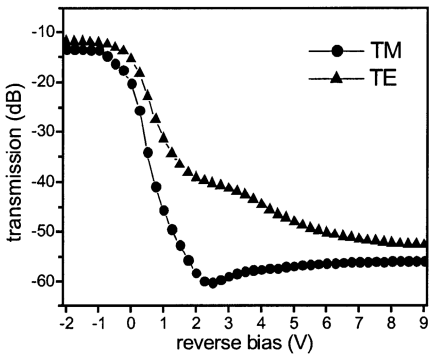

WV2 Fig. 2. Transmission curve as a function of reverse bias.

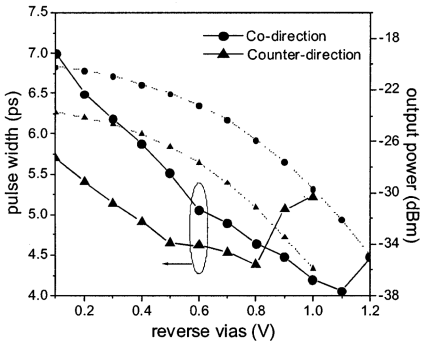

WV2 Fig. 3. Experimental results.

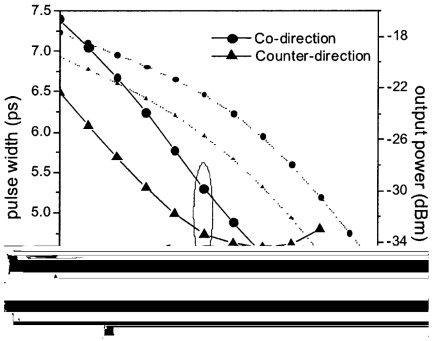

WV2 Fig. 4. Theoretical results.

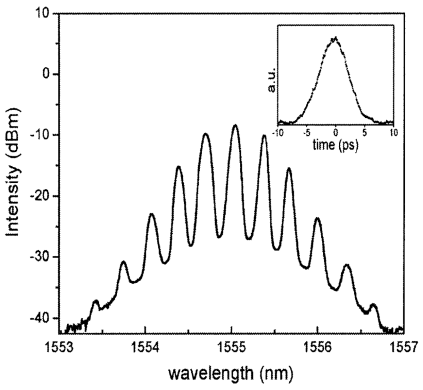

WV2 Fig. 5. Spectrum and autocorrelation trace (insert) at 1V reverse bias.

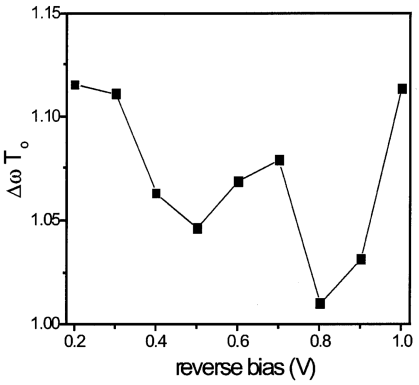

WV2 Fig. 6. spectrum and time product as a function of reverse bias.

is plotted in Fig. 6. It is clear that the chirp of the generated pulses is relatively low.

4. Conclusion

Highly efficient traveling-wave electro-absorption modulators are fabricated with improved multi-quantum well design. The modulation efficiency is as high as 20 dB/V. 40 GHz optical pulses are generated with simple sinusoidal microwave drive. The shortest pulse generated is 4 ps. The experimental co-direction and counter-direction results presented in this works support the theoretical traveling-wave model of operation.

References

1. D. Breuer et al., IEEE Photon. Technol. Lett., Vol. 9, No. 3, pp. 398–400, 1997.
2. M. Suzuki et al, J. Lightwave Technol., Vol. 11, pp. 468–473, 1993.
3. S.Z. Zhang et al., IEEE Photonics Technol. Lett. vol. 11 p. 191, Feb. 1999.
4. S. Oshiba et al, IEEE Journal of Quantum Elec. vol. 34, Feb. 1998.
5. K. Wakita et al, 10th Int. Conf. on Indium Phosphide and Related Materials, May 1998.

WV3 **4:45 pm**

Low insertion loss and polarization-insensitive InP-based Mach-Zehnder modulator for 40 Gbit/s optical regeneration

A. Shen, J. Damon-Lacoste, M. Le Pallec, C. Duchet, J-L. Gentner, F. Devaux, and M. Renaud, *Alcatel Research and Innovation, Route de Nozay, 91460 Marcoussis, France, Email: alexandre.shen@alcatel.fr*

1. Introduction

Polarization independent Mach-Zehnder (MZ) interferometer has been proven to be a key element for synchronous regenerated transmission systems:[1] amplitude and phase modulation can be monitored separately in a MZ, and this provides efficient timing jitter reduction, thus completing the retiming function of in-line 3R regenerators. However, MZ devices reported in literature exhibited 16 dB insertion loss[2] in directional coupler switch applications, or 13 dB in high bit-rate transmission systems.[3] To be cost effective and in the view of an implementation in real systems, a MZ modulator should fulfill stringent system requirement including very low optical insertion loss (<10 dB), high extinction ratio (>6 dB), relatively low phase modulation (<20 deg over one timing period) and very low TE/TM polarization sensitivity (<1 dB).

In this paper, we report the design, fabrication, and experimental results of MZ modulator chips achieving all the above requirements.

2. Chip design, fabrication and characterization

Analysis of the various contributions in the total insertion losses in previous all-active MZ modules based on deep ridge waveguides showed that amongst the fiber to chip coupling losses, the multi-mode interference couplers (MMI) losses and the propagation losses, the most important loss value comes from the fiber to component loss. Under these conditions, the most difficult part of the module fabrication was the fiber to chip facet coupling, which needed special lensed fibers with a small mode diameter as reported in Duchet et al.[4]

Fiber to modulator facet loss can be significantly decreased using a spot size converter (SSC) which has a tapered form (see figure 1). However, efficient SSC stage needs a passive material with lower refractive index (InGaAsP with luminescence wavelength at 1.05 μm) so that the guided mode in the semiconductor material be large enough to match with fiber mode. This requires the butt coupling between the active material (InGaAsP luminescing at 1.43 μm) and the passive material be optimized. For each fiber mode diameter, the sum of the fiber to facet coupling loss, and the butt coupling loss was minimized by readjusting the passive waveguide parameters, namely the InGaAsP layer thickness and the waveguide width, while the butt coupling width has been kept constant and equal to 4 μm.

All this optimization has been carried out by calculating the optical modes in the different waveguides, with the loss value taken as the overlap integral of the modes. The active waveguide width and thickness have been chosen to be 2 μm and 0.3 μm, respectively. Fiber to facet coupling tolerance is defined as the x-and-y off-axis mean value when the coupling is degraded by 1 dB. From figure 2 showing the coupling tolerance versus optical loss, it can be seen that highly tolerant fiber to component coupling results in high insertion loss. Considering the first parameter as predominant to get high yield in module fabrication, a coupling fiber with 6 μm mode diameter

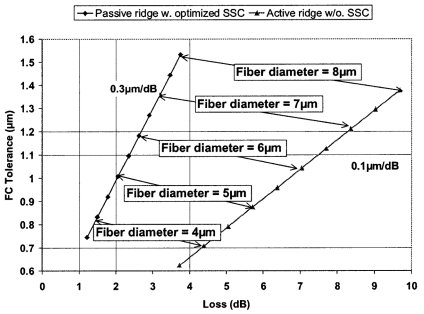

WV3 Fig. 2. Choice of the best fiber diameter and the best output ridge structure. Trade off between fiber coupling (FC) tolerance versus optical losses (FC and butt-coupling), based on calculation.

was chosen as the optimal tradeoff between coupling and butt joint losses (4 dB decrease with respect to active guide without SSC, see figure 2) and the fiber to component coupling tolerance (near 1.2 μm at 1 dB penalty). In reality, SSC exhibits more loss than the calculated values, which is mainly due to the non ideal shape of the butt coupling.

Table 1 lists the measured values of the different optical loss contributions. Reactive Ion Etching has been performed to fabricate the deep ridges, and the fabrication of the multi-mode interference coupler (MMI) has been optimized. As can be seen in figure 3, the optical loss due to MMI width variation is plotted using formulae of reference.[5] The measured excess losses are attributed to scattering losses which have not been accounted for in the calculations. Under this condition, special attention has been paid during the ridge fabrication. Polyimide is then used to allow Ti/Au electrode deposition ontop the ridge structure. The total depth of the final ridge equals 4 μm. The chips are then cleaved, antireflection coated and mounted on special AlN microstriped sub-mount, and electrodes are bound to the support by Au micro strings (figure 1b).

During all the design and fabrication process, the polarization sensitivity was carefully monitored since, in contrast to optical source applications,[6] synchronous 3R in-line regeneration requires less than 1 dB difference in the TE and TM transmission response. A previous study[4] has

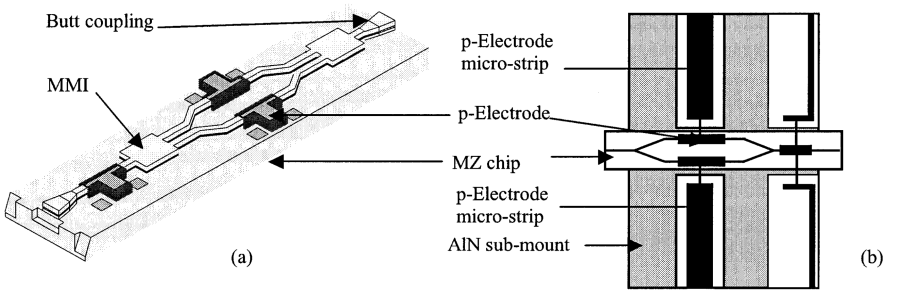

WV3 Fig. 1. Schematic of the MZ modulator (a) and schematic of the chip mounted on its AlN sub-mount.